PROBLEMY MECHATRONIKI
UZBROJENIE, LOTNICTWO, INŻYNIERIA BEZPIECZEŃSTWA

ISSN 2081-5891

7, 4 (26), 2016, 67-84

PROBLEMS IN MECHATRONICS
ARMAMENT, AVIATION, SAFETY ENGINEERING

Impact of Controller Performance on the Process of Guiding an Armour-Piercing Missile onto a Ground-Based Target

Łukasz NOCOŃ, Konrad STEFAŃSKI*

Kielce University of Technology, Faculty of Mechatronics and Mechanical Engineering,
7 1000-lecia PP Av., 25-314 Kielce, Poland
**Corresponding author's e-mail address: stefan5@interia.pl*

Received by the editorial staff on 1 July 2014.
The reviewed and verified version was received on 21 April 2016.

DOI 10.5604/01.3001.0009.5020

Abstract: This work presents an analysis of guiding an anti-tank missile (ATGM) onto a ground-based target. The concept presented here is the feasibility of bypassing obstacles in the path of an ATGM when the obstacle coordinates are known prior to firing the ATGM weapon. The ATGM contemplated here uses a homing algorithm to calculate the stages of the ATGM flight path with the use of polynomial curves (including third-degree polynomial curves). The start and end coordinates of the polynomial curves are determined by the position of the obstacle(s) along the flight path. A method is presented for calculating the factors of subsequent flight path stages, along with a method of equating the ATGM kinematics and dynamics. A comparison is made between the operating efficiency of various configurations of a traditional proportional integral derivative (PID) controller, and at various gain factor values of the PID controller stages. The applied mathematical model of the ATGM are used in a series of numerical simulations for different take-off and in-flight conditions of the projectile. The simulation results are presented in a graphical form.

Keywords: mechanical engineering, anti-tank guided missile, target, homing, controller

This work has been compiled from the paper presented during the 10th International Armament Conference on "Scientific Aspects of Armament and Safety Technology", Ryn, Poland, September 15–18, 2014.

1. INTRODUCTION

The suitable selection of a controller and its settings are of major importance to the performance of the controlled equipment. This selection conditions the response time of the controlled object and the execution of its programmed (pre-set) motion. The controller measures the offset values between the pre-set values and actual values of execution in order to reduce the offsets to negligible values.

The controlled object here is a simplified mathematical model of an anti-tank guided missile (ATGM) moving in a three dimensional space and guided onto its target according to a control algorithm [1], [2]. The algorithm selected for this model is based on third-degree polynomial curves, which are used to calculate the programmed flight path of the ATGM. The control factor of the ATGM is the control force, Q. In computer simulations, the control force emulates the lift from the air passing over the control surfaces of the ATGM while in flight [3], [4]. The control forces were determined using a traditional PID controller. If the missile flight velocity is low, a more efficient gas-dynamic control system may be required [5].

2. MATHEMATICAL MODEL

The dynamic and kinematic equations were derived from the coordinate systems shown in the figure below.

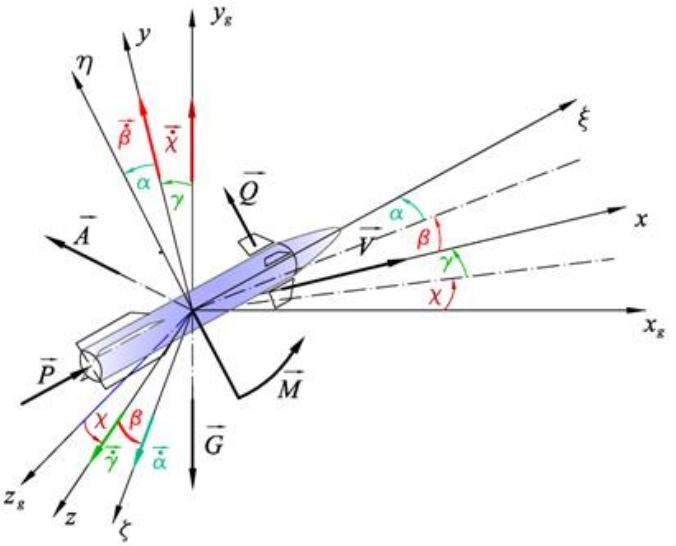

Fig. 1. The ATGM with the assumed coordinate systems

Fig. 1 legend: $Sx_gy_gz_g$ – a coordinate system with the ATGM as the origin and parallel to the launch system; $S\xi\eta\zeta$ – a coordinate system with the ATGM as the origin and formed by rotation of the coordinate system $Sx_gy_gz_g$ by angles ψ, ϑ and φ (respectively: yaw, pitch and roll, in [rad]); *Sxyz*– a velocity coordinate system related to the air stream flows generated by rotation of the coordinate system $Sx_gy_gz_g$ by angles γ and χ and (ATGM flight angles, in [rad]); α, β, – respectively: attack angle and sideslip angle, in [rad]; $\vec{G}$ – gravity force vector; $\vec{V}$ – ATGM velocity vector; $\vec{Q}$ – control force vector; $\vec{M}$ – vector of the total moments of force acting on the ATGM; $\vec{P}$ – rocket engine thrust vector; $\vec{A}$ – vector of the resultant of aerodynamic forces.

Given the assumption that the ATGM is a non-deformable body with a constant mass [6], without rotation around its centreline (φ = 0), and moving in dense atmospheric layers (i.e. right above the ground), the ATGM flight dynamics equations can be defined by the following relations, [7][8][9]:

$$\frac{dV_p}{dt} = \frac{P}{m}\cos\alpha\cos\beta - g\sin\gamma - \lambda_X {V_p}^2 \tag{1a}$$

$$\frac{d\gamma}{dt} = \frac{P}{mV_p}\sin\alpha - \frac{g}{V_p}\cos\gamma + \lambda_Y {V_p}^2\alpha + \frac{Q_y}{mV_p} \tag{1b}$$

$$\frac{d\chi}{dt} = \left(\frac{P}{m}\cos\alpha\sin\beta - \lambda_Z V_p^2\beta - \frac{Q_z}{m}\right)\frac{1}{V_p\cos\gamma} \tag{1c}$$

$$\dot{\omega}_\zeta - \left(\frac{J_{ok}}{J_k} - 1\right)\omega_\xi\omega_\eta = -D_1\frac{V_p^2}{L}\alpha - D_2V_p\frac{d\alpha}{dt} - D_3V_p\frac{d\vartheta}{dt} + \frac{M_{Q\zeta}}{J_k} \tag{1d}$$

$$\dot{\omega}_\eta + \left(\frac{J_{ok}}{J_k} - 1\right)\omega_\xi\omega_\zeta = -D_1\frac{V_p^2}{L}\beta - D_2V_p\frac{d\beta}{dt} - D_3V_p\frac{d\psi}{dt} - \frac{M_{Q\eta}}{J_k} \tag{1e}$$

$$\omega_\xi = \frac{d\varphi}{dt} + \frac{d\psi}{dt}\sin\vartheta \tag{1f}$$

$$\omega_\eta = \frac{d\psi}{dt}\cos\varphi\cos\vartheta + \frac{d\vartheta}{dt}\sin\varphi \tag{1g}$$

$$\omega_\zeta = -\frac{d\psi}{dt}\sin\varphi\cos\vartheta + \frac{d\vartheta}{dt}\cos\varphi \tag{1h}$$

$$\lambda_x = c_x\frac{\rho}{2m}S \qquad \lambda_y = c_y\frac{\rho}{2m}S_y \qquad \lambda_z = c_z\frac{\rho}{2m}S_z \tag{1i}$$

$$D_1 = \frac{C_1L}{J_k} \qquad D_2 = \frac{C_2L}{J_k} \qquad D_3 = \frac{C_3L}{J_k} \tag{1j}$$

with:
m – ATGM mass [kg];
J_k, J_{ok} – ATGM's main central moments of inertia relative to its centreline and transverse axis [kgm^2];
L – ATGM body length [m];
P – rocket engine thrust [N];
V_p – ATGM velocity [m/s];
Q_y, Q_z, – ATGM flight control forces [N],
$M_{Q\zeta}$, $M_{Q\eta}$, – moments imposed by the flight control forces [Nm];
λ_x, λ_y, λ_z, $D_{1,2,3}$ – relative aerodynamic factors of force and moment [1/m] [6];
ω_ξ, ω_η, ω_ζ – ATGM body angular velocities [rad/s];
c_x, c_y, c_z – aerodynamic force factors;
$C_1 = M_z^\alpha = M_y^\beta$ – lift and drift moment factors;
$C_2 = M_z^{\dot\alpha} = M_y^{\dot\beta}$, $C_3 = M_z^{\dot\vartheta} = M_y^{\dot\psi}$ – damping moment factors from the ATGM body angular velocities;
$S = \frac{\pi d^2}{4}$ [m^2];
d – largest cross-sectional diameter of the ATGM [m];
S_y, S_z – lift and drift surface areas [m^2];
ρ – air density [kg/m^2];
g – gravitational acceleration [m/s^2];
t – time [s].

The angles of attack and sideslip are determined by the relation:

$$\alpha = \arctan\left(-\frac{V_\eta}{V_\xi}\right), \qquad \beta = \arcsin\left(\frac{V_\zeta}{V_p}\right) \tag{2a}$$

$$V_\xi = V_p\left(\cos\vartheta\cos\psi\cos\gamma\cos\chi + \sin\vartheta\sin\gamma + \cos\vartheta\sin\psi\sin\chi\right) \tag{2b}$$

$$V_\eta = V_p\left[\left(\cos\vartheta\sin\gamma - \cos\gamma\sin\chi\sin\vartheta\sin\psi\right) - \cos\gamma\cos\chi\sin\vartheta\cos\psi\right] \tag{2c}$$

$$V_\zeta = V_p\left(\cos\gamma\cos\chi + \cos\gamma\sin\chi\cos\psi\right) \tag{2d}$$

with: V_ξ, V_η, V_ζ– velocity vector projections on the bound system axes [m/s].
The moments from the ATGM flight control forces are formulated as follows:

$$M_{Q\zeta} = Q_y \cdot e, \qquad M_{Q\eta} = Q_z \cdot e \tag{3}$$

with: e – distance from the control force application point to the ATGM centre of gravity [m].

The homing kinematics, i.e. the equations of target LOS (line of sight) motion are shown below [10]:

$$\frac{dr}{dt} = V_C\left[\cos\gamma_C \cos\varepsilon \cos(\sigma - \chi_C) + \sin\gamma_C \sin\varepsilon\right] - \\ - V_P\left[\cos\gamma \cos\varepsilon \cos(\sigma - \chi) + \sin\gamma \sin\varepsilon\right] \tag{4a}$$

$$\frac{d\varepsilon}{dt} = \frac{V_P\left[\cos\gamma \sin\varepsilon \cos(\sigma - \chi) - \sin\gamma \cos\varepsilon\right]}{r} + \\ - \frac{V_C\left[\cos\gamma_C \sin\varepsilon \cos(\sigma - \chi_C) - \sin\gamma_C \cos\varepsilon\right]}{r} \tag{4b}$$

$$\frac{d\sigma}{dt} = \frac{V_P\left[\cos\gamma \sin(\sigma - \chi)\right] - V_C\left[\cos\gamma_C \sin(\sigma - \chi_C)\right]}{r\cos\varepsilon} \tag{4c}$$

with: ε – target LOS pitch [rad]; σ – target LOS yaw [rad]; γ_c, χ_c – respectively: target velocity vector pitch and yaw [rad]; r – distance of the ATGM to the target [m]; V_c – target velocity [m/s].

The kinematic *g*-loads applied to the ATGM in flight are described by the following relations [6]:

$$n_x = -\left(\frac{\frac{dV_p}{dt}}{g} + \sin\gamma\cos\chi\right) \tag{5a}$$

$$n_y = -\left(\frac{V_p}{g}\frac{d\gamma}{dt}\cos\chi + \cos\gamma\right) \tag{5b}$$

$$n_z = \frac{V_p}{g}\frac{d\chi}{dt} - \sin\gamma\sin\chi \tag{5c}$$

$$n = \sqrt{n_x^2 + n_y^2 + n_z^2}$$

3. CONTROLLER TYPE

The analysis of guiding the ATGM onto the target was based on a traditional proportional integral derivative (PID) controller. The PID controller outputs were the ATGM flight control forces [11], [12]. The offsets on the PID inputs were the differences between the programmed flight control angles and the actual (executed) ATGM flight angles, as well as the differences between the programmed and actual flight elevation and bearing of flight. Hence this PID can be termed a "twin PID" (2xPID).

However, the simulation included cases of shutting down specific stages of the PID controller. The following relations describe the PID controller equations:

$$Q_y = k_{y1}e_y + k_{y2}\frac{de_y}{dt} + k_{y3}\int_{t_0}^{t_k} e_y\,dt + h_{y1}f_y + h_{y2}\frac{df_y}{dt} + h_{y3}\int_{t_0}^{t_k} f_y\,dt \tag{6a}$$

$$Q_z = k_{z1}e_z + k_{z2}\frac{de_z}{dt} + k_{z3}\int_{t_0}^{t_k} e_z\,dt + h_{z1}f_z + h_{z2}\frac{df_z}{dt} + h_{z3}\int_{t_0}^{t_k} f_z\,dt \tag{6b}$$

$$e_y = \gamma^\circ - \gamma, \qquad e_z = \chi^\circ - \chi, \qquad f_y = y - y_P, \qquad f_z = z - z_P \tag{6c}$$

with: e_y, e_z, f_y, f_z, – control offsets; y – programmed ATGM elevation coordinate at a given time [m]; z – programmed ATGM bearing coordinate [m]; y_p – actual ATGM elevation [m]; z_p – actual ATGM bearing coordinate [m]; γ^o, χ^o – programmed ATGM flight angles [rad]; γ, χ – actual ATGM flight angles [rad]; $k_{y1,2,3}$, $k_{z1,2,3}$, $h_{y1,2,3}$, $h_{z1,2,3}$, – gain factors of specific PID controller stages.

4. ATGM HOMING ALGORITHM

A homing algorithm is essential to determine any programmed position and flight angle coordinates of the ATGM. This work applied a method to calculate the specific ATGM flight path stages, expressed as third degree polynomial curves [12], [13]. The start and end points of the polynomial curves were determined by the points which the ATGM must cross in flight. The coordinates of these point were known before launching the ATGM, e.g. from known actual terrain obstacles. The final flight phase passed over the target, which is struck from above. A simplified schematic diagram of attack for the ATGM is shown in Fig. 2.

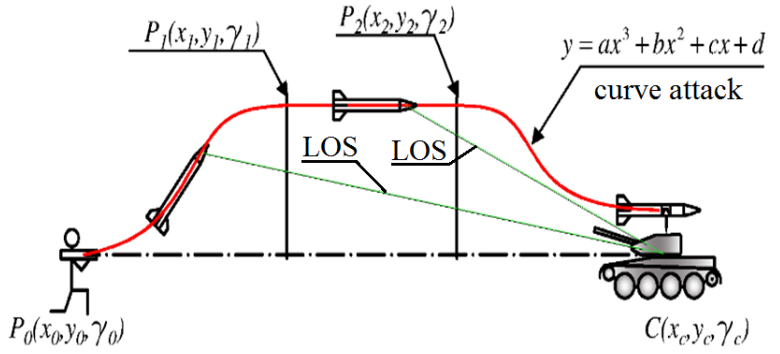

Fig. 2. Simplified schematic diagram of attack for the ATGM, based on the application of polynomial curves

The symbols P_0, P_1 and P_2 in the figure denote the three points the ATGM must reach in flight. The fourth and final point is the target.

The programmed ATGM elevation and bearing coordinates were calculated from a group of relations (7):

$$y = a_{xy}x^3 + b_{xy}x^2 + c_{xy}x + d_{xy}\,, \qquad z = a_{xz}x^3 + b_{xz}x^2 + c_{xz}x + d_{xz} \tag{7}$$

The control angles were calculated as follows:

$$\gamma^\circ = \arctan\left(3a_{xy}x^2 + 2b_{xy}x + c_{xy}\right), \qquad \chi^\circ = \arctan\left(3a_{xz}x^2 + 2b_{xz}x + c_{xz}\right) \tag{8}$$

The equations (7) and (8) feature factors which explicitly defined the forms of the individual third degree polynomial curves used to build the ATGM flight path. The curve values were determined with the following equation systems for both planes of space:

$$\begin{cases} a_{xy}x_0^3 + b_{xy}x_0^2 + c_{xy}x_0 + d_{xy} = y_0 \\ 3a_{xy}x_0^2 + 2b_{xy}x_0 + c_{xy} = \tan(\gamma_0) \\ a_{xy}x_k^3 + b_{xy}x_k^2 + c_{xy}x_k + d_{xy} = y_k \\ 3a_{xy}x_k^2 + 2b_{xy}x_k + c_{xy} = \tan(\gamma_k) \end{cases} \tag{9a}$$

$$\begin{cases} a_{xz}x_0^3 + b_{xz}x_0^2 + c_{xz}x_0 + d_{xz} = z_0 \\ 3a_{xz}x_0^2 + 2b_{xz}x_0 + c_{xz} = \tan(\chi_0) \\ a_{xz}x_k^3 + b_{xz}x_k^2 + c_{xz}x_k + d_{xz} = z_k \\ 3a_{xz}x_k^2 + 2b_{xz}x_k + c_{xz} = \tan(\chi_k) \end{cases} \tag{9b}$$

with: x_0, y_0, z_0 – polynomial curve start coordinates [m];

x_k, y_k, z_k – polynomial curve end coordinates [m];

γ_0, χ_0 – values of programmed ATGM flight angles at curve start [rad];

γ_k, χ_k – values of programmed ATGM flight angles at curve end [rad].

Now the matrix equations can be characterized as:

$$\begin{bmatrix} a_{xy} \\ b_{xy} \\ c_{xy} \\ d_{xy} \end{bmatrix} = \begin{bmatrix} x_0^3 & x_0^2 & x_0 & 1 \\ 3x_0^2 & 2x_0 & 1 & 0 \\ x_k^3 & x_k^2 & x_k & 1 \\ 3x_k^2 & 2x_k & 1 & 0 \end{bmatrix}^{-1} \cdot \begin{bmatrix} y_0 \\ \tan(\gamma_0) \\ y_k \\ \tan(\gamma_k) \end{bmatrix} \tag{10a}$$

$$\begin{bmatrix} a_{xz} \\ b_{xz} \\ c_{xz} \\ d_{xz} \end{bmatrix} = \begin{bmatrix} x_0^3 & x_0^2 & x_0 & 1 \\ 3x_0^2 & 2x_0 & 1 & 0 \\ x_k^3 & x_k^2 & x_k & 1 \\ 3x_k^2 & 2x_k & 1 & 0 \end{bmatrix}^{-1} \cdot \begin{bmatrix} z_0 \\ \tan(\chi_0) \\ z_k \\ \tan(\chi_k) \end{bmatrix} \tag{10b}$$

Once these relations are solved, the determined factors have the following forms:

$$\begin{aligned} a_{xy} &= -\frac{2y_k - 2y_0 + (x_0 - x_k)(\tan(\gamma_k) + \tan(\gamma_0))}{(x_k - x_0)^3} \\ b_{xy} &= \frac{\tan(\gamma_0) - \tan(\gamma_k) - (3x_0^2 - 3x_k^2)a_{xy}}{2x_0 - 2x_k} \\ c_{xy} &= \tan(\gamma_k) - 3x_k^2 a_{xy} - 2x_k b_{xy} \\ d_{xy} &= y_k - x_k^3 a_{xy} - x_k^2 b_{xy} - x_k c_{xy} \end{aligned} \tag{11a}$$

$$\begin{aligned} a_{xz} &= -\frac{2z_k - 2z_0 + (x_0 - x_k)(\tan(\chi_k) + \tan(\chi_0))}{(x_k - x_0)^3} \\ b_{xz} &= \frac{\tan(\chi_0) - \tan(\chi_k) - (3x_0^2 - 3x_k^2)a_{xz}}{2x_0 - 2x_k} \\ c_{xz} &= \tan(\chi_k) - 3x_k^2 a_{xz} - 2x_k b_{xz} \\ d_{xz} &= z_k - x_k^3 a_{xz} - x_k^2 b_{xz} - x_k c_{xz} \end{aligned} \tag{11b}$$

These factors are presented as cascading, i.e. each next factor is determined by those preceding it. If the target is in motion, the coordinate values for the ATGM final flight stage must be calculated in real time, since the relevant curve end point changes position over time. The angle values γ_k and χ_k are calculated as mean values from the slopes of the straight lines which connect the start and end points of the current and next trajectories.

5. NUMERICAL SIMULATIONS

The numerical simulations were carried out for several selections of PID settings [14]. The waypoints that the ATGM must reach in flight are shown in Table 1 for each case. Point 6 was the original position of the target moving at a velocity of V_c = 30 [km/h] and an angle of χ_c = 20 [deg].

Geometric and mass characteristics assumed for the ATGM:

m = 12.9 [kg]; L = 11 [m]; J_k = 1.53 [kgm^2]; J_{ok} = 0.0324 [kgm^2];

D_1 = 0.081 [1/m]; D_2 = 0.0821 [1/m]; D_3 = 0.00041 [1/m];

λ_x = 0.000171 [1/m]; $\lambda_y = \lambda_z$ = 0.051 [1/m]; d= 0.12 [m], e = 0.45 [m].

ATGM rocket engine thrust values assumed: P = 3 500 [N] for a flight duration of t < 0.5 [s] and P = 400 [N] for a flight duration of t >0.5 [s]. The values of the PID controller gain factors were selected using the algorithm defined in [14]

Table 1. ATGM in-flight waypoint coordinates

Waypoint no.	x [m]	y [m]	z [m]
1	50	5	0
2	150	20	30
3	250	10	-30
4	550	5	5
5	750	7	-5
6	1000	0	10

5.1. Case 1: P controller

In this case the PID controller had the integral and derivative stages off-line in both spatial planes, and the input arguments only included the offset values calculated as the difference between the programmed and actual positions of the ATGM. Hence the control forces were:

$$Q_y = h_{y1} f_y \tag{12a}$$

$$Q_z = h_{z1} f_z \tag{12b}$$

Gain values: h_{y1} = 80 000 [N/m] and h_{z1} = 80 000 [N/m]. The numerical simulation results are shown in Figs. 3 to 10.

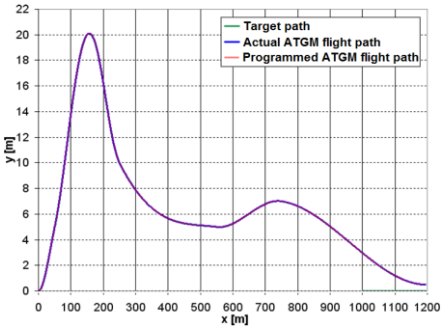

Fig. 3. Programmed vs. actual ATGM flight path and the target path in the vertical plane

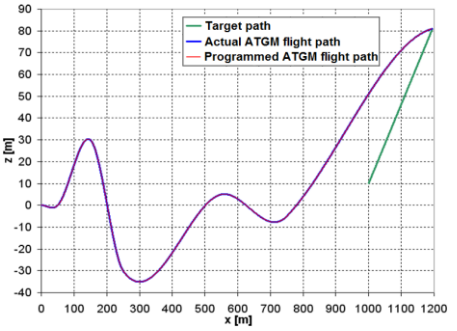

Fig. 4. Programmed vs. actual ATGM flight path and the target path in the horizontal plane

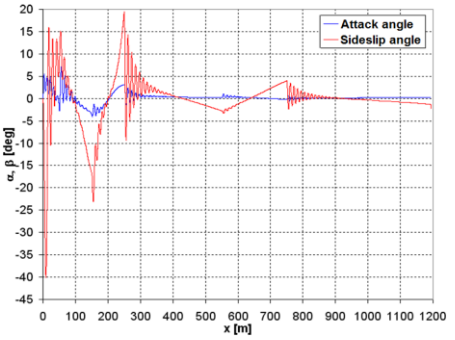

Fig. 5. ATGM in-flight angles of attack and sideslip

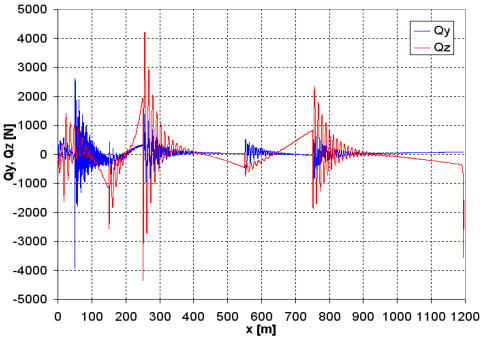

Fig. 6. Control forces in the vertical and horizontal planes

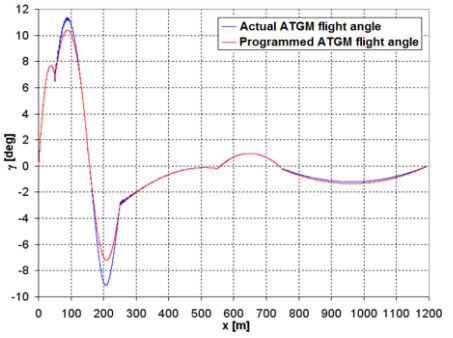

Fig. 7. Programmed vs. actual ATGM flight angle in the vertical plane

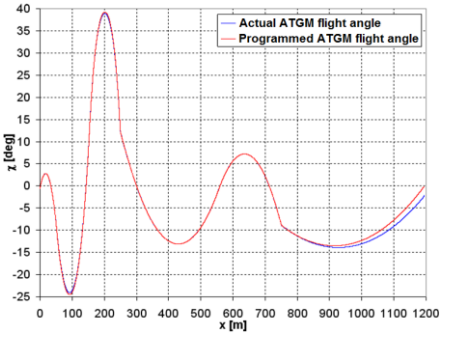

Fig. 8. Programmed vs. actual ATGM flight angle in the horizontal plane

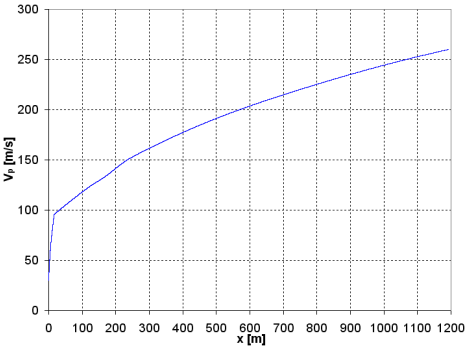

Fig. 9. ATGM in-flight velocity

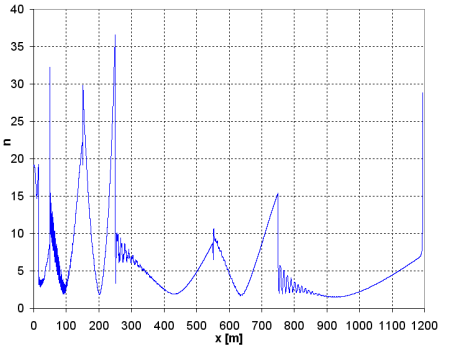

Fig. 10. ATGM in-flight g-loads

5.2. Case 2: 2 × P controller

In this case the PID controller had the integral and derivative stages off-line in both spatial planes; the input arguments were two types of offset, i.e. the difference between the programmed and actual ATGM position, and the difference between the programmed and actual ATGM flight angles. The control forces were:

$$Q_y = k_{y1} e_y + h_{y1} f_y \tag{13a}$$

$$Q_z = k_{z1} e_z + h_{z1} f_z \tag{13b}$$

Gain values: k_{y1} = 80 000 [N/rad], k_{z1} = 800 000 [N/rad], h_{y1} = 80 000 [N/m] and h_{z1} = 800 000 [N/m]. The numerical simulation results for these PID settings are shown in Figs. 11 to 18.

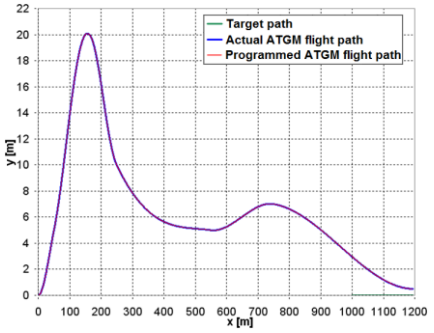

Fig. 11. Programmed vs. actual ATGM flight path and the target path in the vertical plane

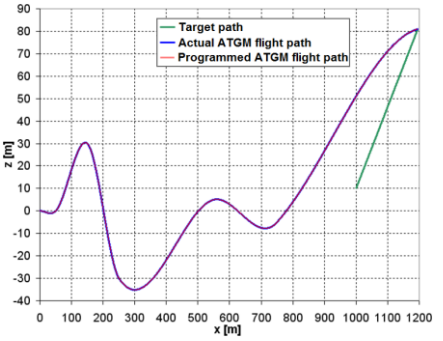

Fig. 12. Programmed vs. actual ATGM flight path and the target path in the horizontal plane

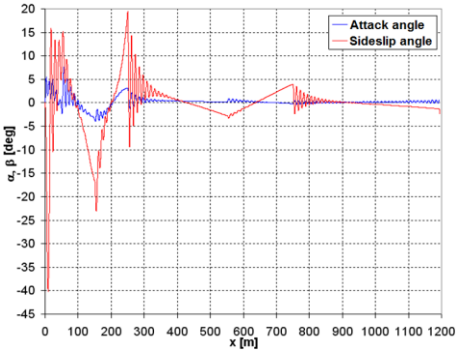

Fig. 13. ATGM in-flight angles of attack and sideslip

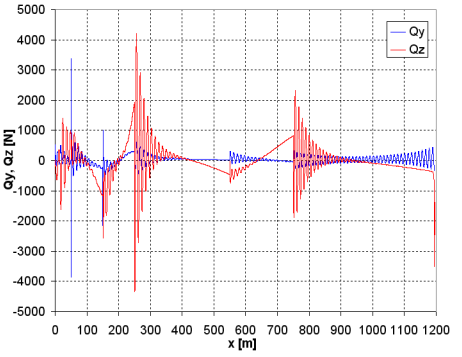

Fig. 14. Control forces in the vertical and horizontal planes

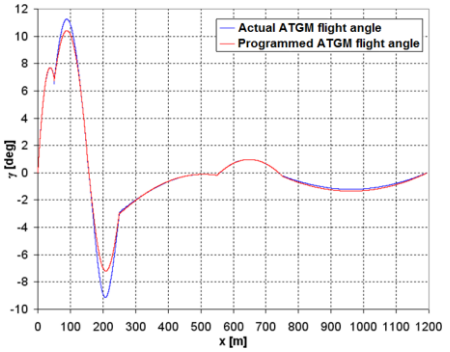

Fig. 15. Programmed vs. actual ATGM flight angle in the vertical plane

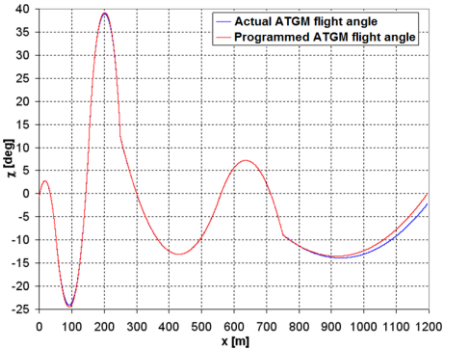

Fig. 16. Programmed vs. actual ATGM flight angle in the horizontal plane

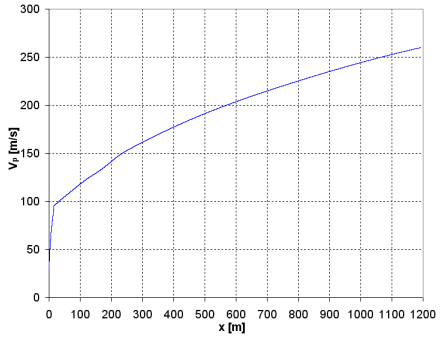

Fig. 17. ATGM in-flight velocity

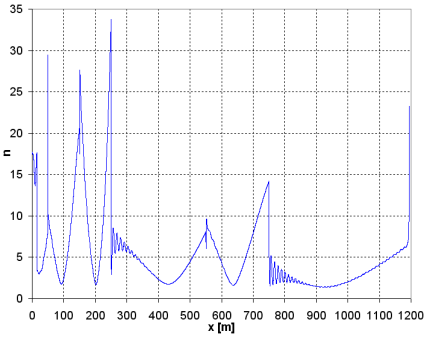

Fig. 18. ATGM in-flight *g*-loads

5.3. Case 3: PID controller

In this case the PID controller had all stages on-line in both spatial planes, and the input arguments only included the offset values calculated as the difference between the programmed and actual positions of the ATGM. The control forces were:

$$Q_y = h_{y1} f_y + h_{y2} \frac{df_y}{dt} + h_{y3} \int_{t_0}^{t_k} f_y \, dt \tag{14a}$$

$$Q_z = h_{z1} f_z + h_{z2} \frac{df_z}{dt} + h_{z3} \int_{t_0}^{t_k} f_z \, dt \tag{14b}$$

Gain values: h_{y1} = 900 [N/m], h_{z1} = 900 [N/m], h_{y2} = 50 [Ns/m], h_{z2} = 50 [Ns/m], h_{y3} = 2 500 [N/ms] and h_{z3} = 2 500 [N/ms]. The numerical simulation results for these PID settings are shown in Figs. 19 to 26.

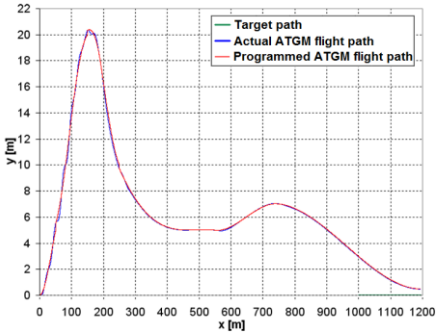

Fig. 19. Programmed vs. actual ATGM flight path and the target path in the vertical plane

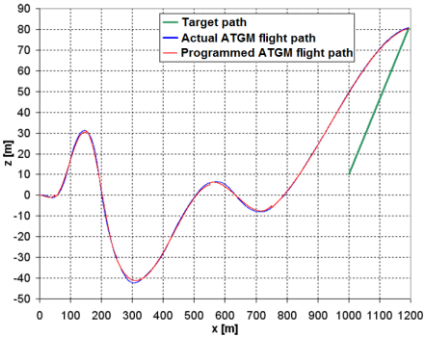

Fig. 20. Programmed vs. actual ATGM flight path and the target path in the horizontal plane

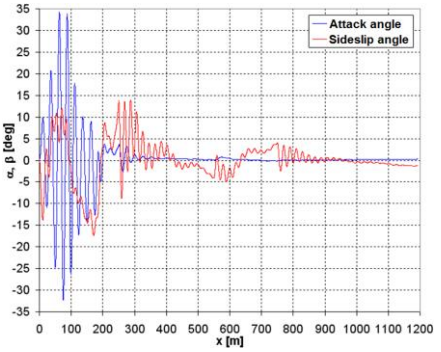

Fig. 21. ATGM in-flight angles of attack and sideslip

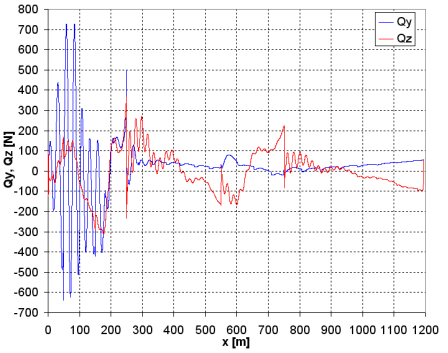

Fig. 22. Control forces in the vertical and horizontal planes

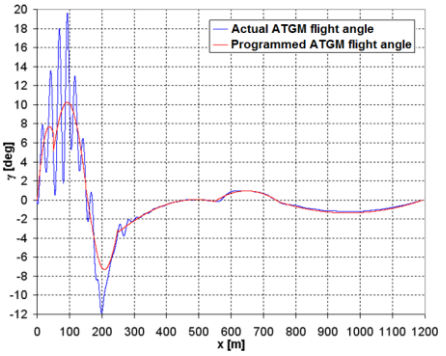

Fig. 23. Programmed vs. actual ATGM flight angle in the vertical plane

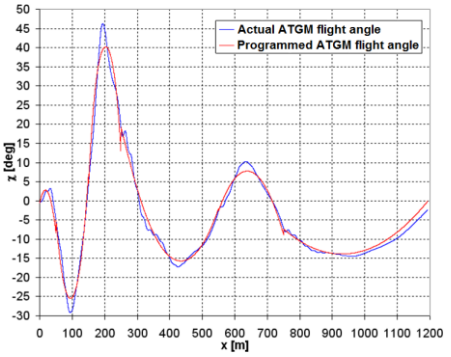

Fig. 24. Programmed vs. actual ATGM flight angle in the horizontal plane

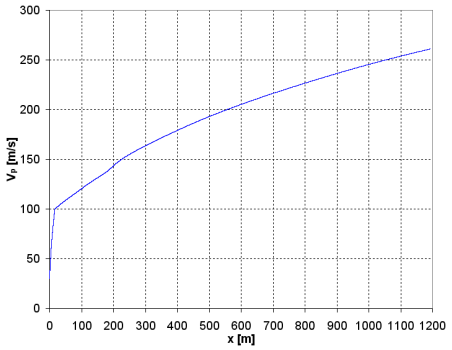

Fig. 25. ATGM in-flight velocity

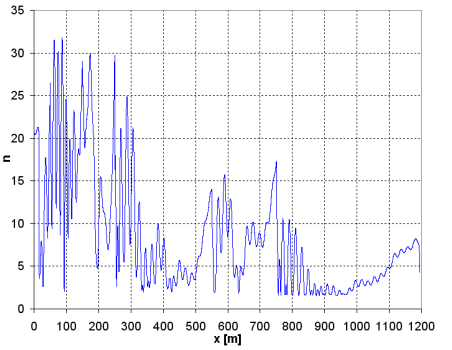

Fig. 26. ATGM in-flight g-loads

5.4. Case 4: 2 × PID controller

In this case the PID controller had all stages online in both spatial planes; the input arguments were two types of offset, i.e. the difference between the programmed and actual ATGM positions, and the difference between the programmed and actual ATGM flight angles. The control forces were:

$$Q_y = k_{y1}e_y + k_{y2}\frac{de_y}{dt} + k_{y3}\int_{t_0}^{t_k} e_y\,dt + h_{y1}f_y + h_{y2}\frac{df_y}{dt} + h_{y3}\int_{t_0}^{t_k} f_y\,dt \tag{15a}$$

$$Q_z = k_{z1}e_z + k_{z2}\frac{de_z}{dt} + k_{z3}\int_{t_0}^{t_k} e_z\,dt + h_{z1}f_z + h_{z2}\frac{df_z}{dt} + h_{z3}\int_{t_0}^{t_k} f_z\,dt \tag{15b}$$

Gain values: k_{y1} = 400 [N/rad], k_{z1} = 300 [N/rad], k_{y2} = 320 [Ns/rad], k_{z2} = 470 [Ns/rad], k_{y3} = 10 [N/rads], k_{z3} = 20 [N/rads], h_{y1} = 900 [N/m], h_{z1} = 700 [N/m], h_{y2} = 36 [Ns/m], h_{z2} = 14 [Ns/m], h_{y3} = 2300 [N/ms] and h_{z3} = 500 [N/ms]. The numerical simulation results for these PID settings are shown in Figs. 27 to 34.

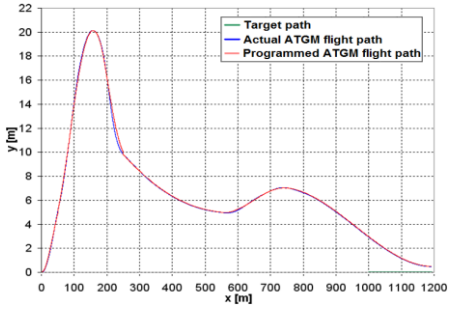

Fig. 27. Programmed vs. actual ATGM flight path and the target path in the vertical plane

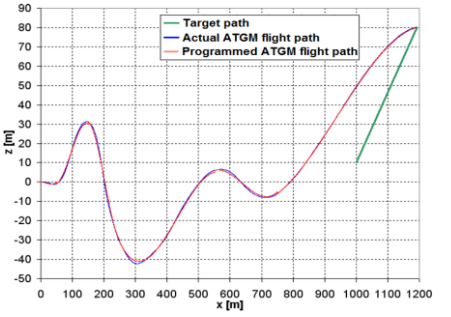

Fig. 28. Programmed vs. actual ATGM flight path and the target path in the horizontal plane

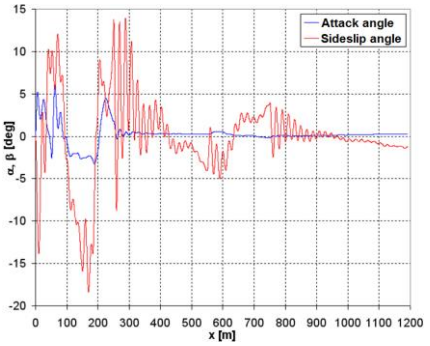

Fig. 29. ATGM in-flight angles of attack and sideslip

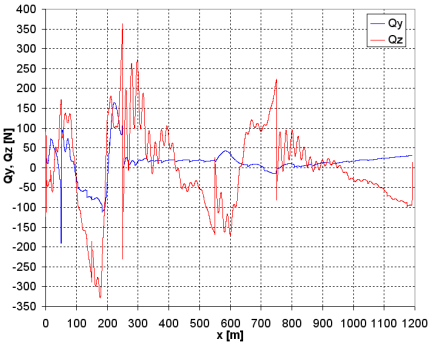

Fig. 30. Control forces in the vertical and horizontal planes

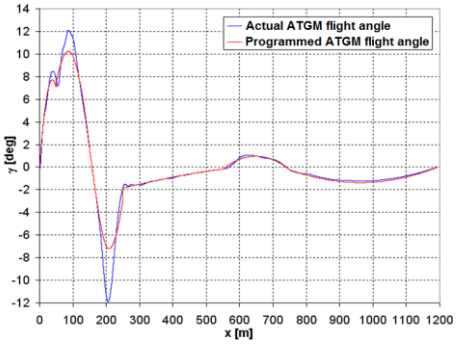

Fig. 31. Programmed vs. actual ATGM flight angle in the vertical plane

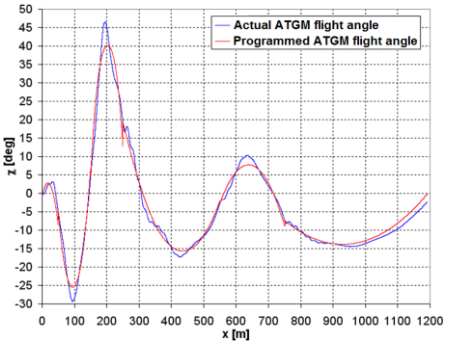

Fig. 32. Programmed vs. actual ATGM flight angle in the horizontal plane

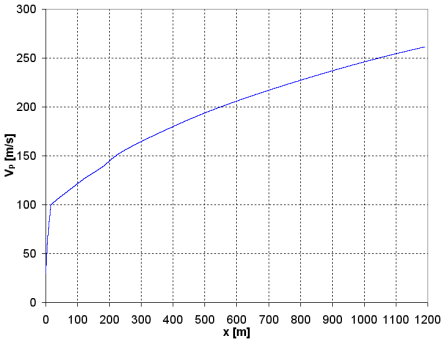

Fig. 33. ATGM in-flight velocity

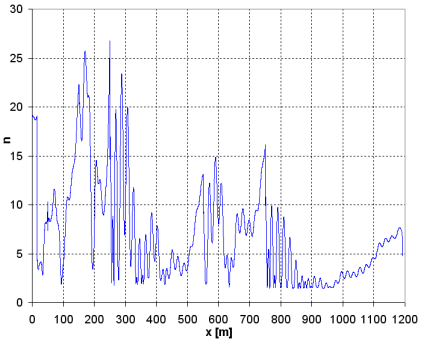

Fig. 34. ATGM in-flight g-loads

6. SUMMARY

The numerical simulations indicate that the application of a specific controller configuration is highly critical in the determination of the flight control forces for an anti-tank guided missile. In the first simulated case (1 × P), the programmed and actual flight paths coincided in both spatial planes. The charts of the ATGM flight angles also indicate that this control configuration is smooth. However, the results were only satisfactory at extremely high gain factors, which are impossible to generate in real life conditions. Therefore, the control force values are also extremely high and unrealistic. Adding a second P stage (see case no. 2) reduced the control forces, especially in the vertical plane; however, the values remained extremely high with equally extreme and unrealistic gain factors. Case no. 3 had all PID stages on-line; however, with the input offset calculated only as the difference between the programmed and actual ATGM positions, the differences between the programmed and actual flight angles were significant, especially in the first stage of flight. Here the control forces were much lower than in the two previous cases, although the values remained relatively high. Only the fully enabled 2 × PID controller (case no. 4) provided acceptable control force values, as concluded from a cross-reference with [15]. The values for the angles of attack and sideslip were also satisfactory. A drawback of the applied homing algorithm is that high pitching of the control forces occur at the concatenation points of the flight trajectory, which is a phenomenon more pronounced in proportional controllers. The pitching is caused by the discontinuity between the angular velocities $\frac{d\gamma}{dt}$ and $\frac{d\chi}{dt}$. This poses a problem which warrants a solution yet to be solved.

REFERENCES

[1] Harris John, Nathan Slegers. 2009. “Performance of a fire-and-forget anti-tank missile with a damaged wing”. *Mathematical and computer modelling* 50 (7) : 292-305.

[2] Evans David M. 1990. “The direct-fire anti-armour capability of UK land forces”. *Intern. Defense Review* 07/1990: 739-742.

[3] Koruba Zbigniew, Edyta Ładyżyńska-Kozdraś. 2010. “The dynamic model of a combat target homing system of an unmanned aerial vehicle”. *Journal of Theoretical and Applied Mechanics* 48 (3) : 551-566.

[4] Krzysztofik Izabela. 2012. “The dynamics of the controlled observation and tracking head located on a moving vehicle”. *Solid State Phenomena* 180 : 313-322.

[5] Baranowski Leszek, Bogdan Machowski. 2011. „Analiza efektywności metody proporcjonalnej nawigacji w sterowaniu gazodynamicznym wirujących obiektów latających". *Problemy mechatroniki. Uzbrojenie, lotnictwo, inżynieria bezpieczeństwa – Problems of Mechatronics. Armament, Aviation, Safety Engineering* 2 (1) : 37-54.

[6] Koruba Zbigniew, Jan W. Osiecki. 1999. *Budowa, dynamika i nawigacja pocisków rakietowych bliskiego zasięgu*. Kielce: Wydawnictwo Politechniki Świętokrzyskiej.

[7] Stefański Konrad, Zbigniew Koruba. 2012. "Analysis of the guiding of bombs and ground targets using a gyroscope system". *Journal of Theoretical and Applied Mechanics* 50 (4) : 967-973.

[8] Koruba Zbigniew, Janusz Tuśnio. 2011. „Koncepcja i algorytm manewru ochrony obiektu latającego przed kolizją z napowietrzną linią przesyłową wysokiego napięcia". *Problemy mechatroniki. Uzbrojenie, lotnictwo, inżynieria bezpieczeństwa – Problems of Mechatronics. Armament, Aviation, Safety Engineering* 2 (4) : 69-80.

[9] Gapiński Daniel, Zbigniew Koruba, Izabela Krzysztofik. 2012. "The model of dynamics and control of a modified optical scanning seeker in anti-aircraft rocket missile". *Mechanical Systems and Signal Processing* 45 (4) : 433-447.

[10] Ładyżyńska-Kozdraś Edyta, Zbigniew Koruba. 2012. "Model of the final navigation section of a self-guided missile steered by a gyroscope". *Journal of Theoretical and Applied Mechanics* 50 (2) : 473-485.

[11] Koruba Zbigniew, Łukasz Nocoń. 2012. „Wybrane algorytmy automatycznego naprowadzania przeciwpancernego pocisku rakietowego atakującego cel z górnego pułapu". *Pomiary Automatyka Robotyka* 2/2012: 398-403.

[12] Koruba Zbigniew, Łukasz Nocoń. 2013. „Automatyczne sterowanie przeciwpancernym pociskiem rakietowym oparte na funkcjach wielomianowych". *Zeszyty Naukowe Politechniki Opolskiej*, *Mechanika* 101 (348) : 24.1-24.19.

[13] Koruba Zbigniew, Zbigniew Dziopa, Izabela Krzysztofik. 2010. "Dynamics and control of a gyroscope-stabilized platform in a self-propelled anti-aircraft system". *Journal of Theoretical and Applied Mechanics*, 48(1) : 5-26.

[14] Koruba Zbigniew. 2001. *Dynamika i sterowanie giroskopem na pokładzie obiektu latającego*. Monografie, Studia, Rozprawy no. 25. Kielce: Politechnika Świętokrzyska.

[15] Dziopa Zbigniew. 2013. „Ocena wpływu manewrów obronnych celu na sterowanie rakietą". *Zeszyty Naukowe Politechniki Rzeszowskiej* 288 (85) : 229-238.

Wpływ typu regulatora na proces naprowadzania przeciwpancernego pocisku rakietowego na cel naziemny

Łukasz NOCOŃ, Konrad STEFAŃSKI

Streszczenie. W pracy zaprezentowana została analiza naprowadzania na cel naziemny przeciwpancernego pocisku kierowanego (PPK). Idea polega na możliwości omijania przeszkód przez PPK, których współrzędne są znane przed wystrzeleniem. Rakieta ta ma zaimplementowany algorytm naprowadzania, który polega na obliczaniu odcinków lotu PPK według krzywych wielomianowych (w tej pracy wykorzystano krzywe trzeciego stopnia), których współrzędne początku i końca są wymuszone przez położenie przeszkody lub przeszkód. Zaprezentowany został sposób obliczania współczynników dla kolejnych odcinków toru lotu, jak również równania kinematyki i dynamiki pocisku. Przeprowadzone będzie także porównanie skuteczności działania klasycznego regulatora proporcjonalno-całkująco różniczkującego w różnych konfiguracjach i przy różnych wartościach współczynników wzmocnienia jego poszczególnych członów. Zastosowany model matematyczny PPK posłuży do przeprowadzenia szeregu symulacji numerycznych dla różnych warunków startu i lotu przeciwpancernego pocisku kierowanego. Ich wyniki zostaną przedstawione w postaci graficznej.

Słowa kluczowe: mechanika, przeciwpancerny pocisk kierowany, cel, naprowadzanie, regulator